Finite element analysis of stresses in flexible bulk solid container

Finite element analysis of stresses in flexible bulk solid container

Journal:	*Advances in Structural Engineering*
Manuscript ID	ASE-17-0500.R1
Manuscript Type:	Special Issue for Professor Rotter
Date Submitted by the Author:	12-Feb-2018
Complete List of Authors:	Pantaleev, Stefan; University of Edinburgh School of Engineering, Institute for Infrastructure and the Environment Papanicolopulos, Stefanos-Aldo; University of Edinburgh School of Engineering Ooi, Jin; University of Edinburgh School of Engineering
Keywords:	flexible bulk containers, wall stiffness, wall pressures, bulk stresses, finite element analysis
Abstract:	Current theories and design codes pertaining to storage structures for bulk solids have been developed in the context of rigid-walled silos, and may not be applicable for smaller and highly-flexible containers that are often used for industrial packaging and intermediate storage. The focus of this study is to investigate the effect of wall flexibility on the bulk stresses and wall pressures during storage using finite element analysis. The results show that when the wall stiffness is low, the computed bulk stresses in the vertical bin section are dominated by plasticity, whilst the stresses in the hopper section remain in the elastic state. In this situation the wall pressure in the bin section is heavily influenced by the strength of the stored solid, which controls the extent of plastic flow. Overall, the normal wall pressure in the bin section is found to decrease with wall flexibility leading to a corresponding increase in vertical stress in the stored solid. As a consequence, the stresses in the hopper also increase leading to increasing loads on the hopper walls and potential exacerbation of handling issues for cohesive materials in highly flexible containers.

Finite element analysis of stresses in flexible bulk solid container

Abstract

Current theories and design codes pertaining to storage structures for bulk solids have been developed in the context of rigid-walled silos, and may not be applicable for smaller and highly-flexible containers that are often used for industrial packaging and intermediate storage. The focus of this study is to investigate the effect of wall flexibility on the bulk stresses and wall pressures during storage using finite element analysis. The results show that when the wall stiffness is low, the computed bulk stresses in the vertical bin section are dominated by plasticity, whilst the stresses in the hopper section remain in the elastic state. In this situation the wall pressure in the bin section is heavily influenced by the strength of the stored solid, which controls the extent of plastic flow. Overall, the normal wall pressure in the bin section is found to decrease with wall flexibility leading to a corresponding increase in vertical stress in the stored solid. As a consequence, the stresses in the hopper also increase leading to increasing loads on the hopper walls and potential exacerbation of handling issues for cohesive materials in highly flexible containers.

Key words

Flexible bulk containers, wall pressures, bulk stresses, finite element analysis

1. Introduction

Silos and bunkers made of aluminium, steel or concrete have traditionally been used in industrial operations for storing and processing of bulk materials, and the stresses in these

rigid structures have been studied extensively (e.g. Ooi et al., 1990; Ooi and Rotter, 1990; Rotter, 2001). Janssen's theory (Janssen, 1895) has typically been used to predict the pressures in the vertical (bin) section of a silo while several theories for the pressures in the hopper section have been proposed (Ooi and Rotter, 1991), with Walker's theory (Walker, 1966) being currently adopted in the Eurocodes (EN 1991-4:2006). In industrial plants, Flexible Intermediate Bulk Containers (FIBCs) made of fabric have been used for industrial packaging and intermediate storage solutions. These containers offer significant advantages: they are both lightweight and economical. However, the existing theories adopted in design codes do not take the effect of wall flexibility into consideration and their applicability to FIBCs is questionable. Indeed, the few previous experimental and numerical studies of stresses in flexible silos have all shown that these stresses are not well predicted by the established theories (Goodey et al., 2006; Ooi and Rotter, 1990, 1991) even when considering relatively stiff walls in comparison to those of FIBCs. Furthermore, no studies on the stresses in highly flexible containers such as FIBC's could be identified. Consequently the stresses in such containers appear to be unknown and the appropriate structural and functional design of these containers remains unclear. Consistent with this, both structural problems such as creep and tearing of the wall fabric and operational problems such as non-uniform, incomplete or arrested discharge of cohesive solids have been observed in industry in relation to FIBCs. Such problems lead to loss of productivity in industrial processes and further research is needed to develop an understanding of the stresses in these containers and to inform their design.

A Finite Element (FE) analysis of the effect of wall stiffness on the stresses in a flexible axisymmetric container is carried out in this study. Relatively simple constitutive models

are used to model the complex behaviour of the wall fabric and stored bulk solid. Characteristic values of relevant numerical model parameters for the bulk solid are employed based on the established design codes for silos, while the parameters for the wall are estimated from uniaxial extension tests. The wall flexibility is quantified in terms of the relative stiffness parameter proposed by Ooi and Rotter (Ooi and Rotter, 1990) and a wide range of wall flexibility is explored.

2. Numerical modelling approach

An example of an FIBC can be seen in Figure 1. It is a "buggy" used for the storage and transport of industrial solids within a manufacturing plant. It consists of a rectangular steel frame, on which a polymer-coated fabric composite canvas is suspended to form the container. The canvas is tied at the top of the frame and at an intermediate height to form the vertical bin section of the container, and is tailored in such a way as to form a suspended pyramidal hopper. On filling the container, the canvas deforms significantly and assumes a more complex shape shown in Figure 1. The large deformations arise from the low stiffness of the canvas as well as structural compliance due to a small amount of initial slack in the canvas. In this study we aim to isolate the effect of the wall stiffness and ignore the initial compliance of the canvas by adopting and idealized geometry.

[Insert Figure 1]

While FIBC's are typically of a rectangular plan form geometry similar to the one in Figure 1, the relevant theoretical and design code calculations we aim to evaluate pertain to an axisymmetric geometry. Furthermore, it has been shown that the stress distribution in rectangular containers is highly complex and poorly understood (Goodey et al., 2006) even if the further complexities arising from a very high degree of wall flexibility are not

present. Therefore we focus on the axisymmetric analysis inherent in the design codes as a first step towards understanding the effect of wall flexibility on the stresses in flexible containers.

The geometry adopted in the analysis is shown in Figure 2. The model consists of a cylindrical bin and a conical hopper with dimensions similar to those of the "buggy" in Figure 1. A conical surcharge pile, approximating the free surface of the solid at the end of filling, is included.

[Insert Figure 2]

The boundary conditions used in the analysis reflect those for a flexible container, where the canvas, which forms the wall, is tied to a rigid steel frame at the top and bottom of the vertical bin section (Figure 1).

Only the pressures during storage are considered in this study and therefore a static FE analysis is performed. The filling of the container is modelled by linearly increasing gravity in the model over a single step in the analysis, a commonly adopted approach in previous studies (e.g. Holst et al., 1999). The more sophisticated method of introducing the bulk solid in layers (e.g. Ding et al., 2013) could not be used due to large overlaps between the deformed wall and newly introduced layers of solid.

The non-linear geometric effects in this analysis were found to be negligible and were ignored to minimize computational time. The analysis was carried out using the ABAQUS/Standard software package (Simulia, 2012).

2.1 Modelling the bulk solid

The constitutive laws applied to the granular solid in silo applications have varied widely in complexity (Feise and Schwedes, 1998). These include linear elastic (e.g. Ooi and

Rotter, 1990) and non-linear elastic laws (e.g. Chen et. al, 2001), local elasto-plastic laws (e.g. Link and Elwi, 1990), local visco-plastic laws (e.g. Häussler and Eibl, 1984) as well as more sophisticated non-local hypoplastic laws (e.g. Tejchman, 1998; Wójcik and Tejchman, 2009, 2016). The choice of a constitutive law for the stored solid depends on the phenomena of interest (Feise and Schwedes, 1998). For the prediction of storage and discharge pressures the advantages of complex plasticity laws have been questioned (Nielsen and Wedner, 1998). For static wall pressures in particular, Ooi and Rotter (1990) showed that modelling the complex plasticity of the stored solid did not have advantages over using a simple elastic model, because the structure provided sufficient confinement for the solid to remain predominantly in the pseudo-elastic state. The authors showed the same to be the case in the conical hoppers of steel silos (Ooi and Rotter, 1991). Numerical studies by Ooi et al. (1996) and Chen et al. (2001) further demonstrated that adopting more complex non-linear elastic models such as a hyperbolic or power law models produced effectively the same results for the static wall pressure in steel silos as the simple linear elastic model. However, in the case of a flexible thin-walled steel container Goodey et al., (2003) found that modelling the plasticity of the stored solid did have an effect on the computed wall pressures, because the significant wall deformations allowed for the development of shear zones within the solid. The accurate prediction of such shear zones requires the use of more sophisticated non-local constitutive models (e.g. Tejchman, 2009). However, in the case of the above container a simple local elastic-perfect plastic model for the bulk solid produced a good agreement with experimental wall pressure measurements during storage (Goodey et al., 2006). This is an indication that a more complex model may not be necessary for the study of our

problem- the effect of wall flexibility on static wall pressures. Therefore, we adopt a similar approach to Goodey et al. (2006) and model the stored solid as an elastic/perfectly-plastic material. The plasticity of the solid is modelled with the classic Mohr-Coulomb failure criterion without hardening, the mathematical formulation of which is described in detail elsewhere (Simulia, 2012).

The model parameters adopted in the analysis are shown in Figure 2 – these correspond to characteristic values for limestone powder given by Rotter (2001). Limestone powder was chosen as representative of industrial powders, which are typically stored in "buggies" such as the one in Figure 1.

A characteristic value for the elastic modulus of limestone powder was estimated from AS 3774:1996. It should be noted that the Young's modulus for the stored solid is assumed to be constant in the analysis while in reality the modulus is expected to increase with depth as stress level increases. This has not been considered in this study.

The Poisson's ratio for the material was calculated from the elastic relationship for the lateral pressure ratio in a stiff smooth cylinder (Ooi, 1990; Rotter, 2001):

$$v_S = \frac{K}{K+1} \quad (1)$$

where K is the lateral pressure ratio, calculated here according to the Eurocode for silos (EN 1991-4:2006) as

$$K = 1.1(1 - \sin(\phi)) \quad (2)$$

where φ is the effective angle of internal friction of the material.

The effect of the dilation angle on the predicted wall pressure was explored but found to be negligible within a practical range of values (φ_d<20^0) for all analysis cases. The minimum allowable value (φ_d=1^0) was adopted in the analysis. Similarly to previous

studies, a very small value was adopted for the cohesion intercept to improve numerical stability (Goodey et al., 2006).

2.2 Modelling the wall canvas

The walls of FIBCs are typically made of polymer-coated fabric composites. These materials exhibit a highly complex mechanical behaviour, characterised by stress anisotropy, non-linear plasticity and creep (Hallal et al., 2013; Pargana et al., 2007). Consequently, sophisticated constitutive models, involving a large number of parameters and significant experimental calibration, are required to model these materials accurately (Dinh et al., 2015; Hallal et al., 2013; Pargana et al., 2007). Exploring such complex models is beyond the scope of this study. Instead, the wall of the container is modelled using a linear-elastic isotropic constitutive model as this should be enough to capture the main effect of the wall flexibility on the bulk stresses and the induced loading on the container walls.

[Insert Figure 3]

The elastic modulus for the wall canvas was estimated from uniaxial extension tests on samples from the wall material of the powder buggy shown in Figure 1. The extension tests were performed according to BS EN 1421:1998. Samples were tested in the warp and fill directions of the fabric as well as at 45° to the warp/fill direction. The results are shown in Figure 3 and reveal the low stiffness and high degree of anisotropy of the material. Young's moduli were estimated from a linear fit to the stress-strain curves in each direction (Figure 3) using the data up to 10 MPa tensile stress, which is the computed stress range for the majority of the wall. Within this stress range, a linear

approximation appears to be reasonable. The results are comparable to the values reported by a previous study on a similar material (Dinh et al., 2015).

It should be pointed out that the estimated Young's moduli correspond to a lower bound for the stiffness of the canvas, because fabrics exhibit a pronounced stiffening effect in biaxial tension, which is the realistic loading situation (Dinh et al., 2015; Pargana et al., 2007). In this study, a wide range of elastic moduli was explored, using the estimated wall stiffness in FIBCs as a lower bound and also covering much higher stiffnesses as shown in Figure 2. The Poisson ratio adopted in our analysis is an average value of the ones reported in the abovementioned study of Dinh et al., (2015).

2.3 Modelling the interaction between the bulk solid and the wall

The normal contact at the wall was modelled using hard pressure overclosure with direct enforcement and the frictional traction was modelled using the Coulomb friction model with a penalty enforcement. Both of these are standard options in the Abaqus software (Simulia, 2008). The penalty enforcement for the friction model was used to reduce the excessive computational times required of the direct enforcement of friction (Chen et al., 2001; Simulia, 2008). In this approach, the surface nodes are allowed to slide over a small distance called the elastic slip, before the limiting Coulomb friction is reached. The magnitude of elastic slip controls the friction mobilisation along the contact surfaces and a sufficiently small value should be used to ensure that the numerical results are not affected (Chen et al., 2001; Simulia, 2008). A value of 10^{-7}m was found to produce satisfactory results in a sensitivity test as shown in Figure 4. For all analysis cases in this study, the frictional traction along the wall was fully mobilized everywhere with the exception of a negligibly small region immediately above the outlet.

[Insert Figure 4]

2.4 Mesh convergence

The sensitivity of the numerical results to the number and type of elements adopted in the analysis was assessed. Different mesh densities were considered and both first- and second-order elements for the solid and wall. The numerical results were not significantly affected by the number of elements within the range considered as shown in Fig 5a, with the exception of a large localised pressure peak at the hopper transition as shown in Fig 5b. This peak has been regarded as a numerical artefact and previous researchers have attempted to eliminate it by smoothing the transition region to a curve or a circular arc (Ooi, 1990; Wang et al., 2013) . It can be observed, however, that this locally high pressure has negligible effect on the results away from its neighbouring nodes (Figure 5b) and therefore negligible effect on the computed stresses in the solid and on the walls. A potential explanation is that this pressure, although high, only acts on a very small area of the wall and therefore has a negligible effect on the overall equilibrium calculation. No artificial smoothing of the transition was attempted in this study.

The finest mesh considered was adopted in order to increase the resolution of the computed stress field in the stored solid and the combination of first order axisymmetric quadrilaterals (CAX4) for the solid and second-order axisymmetric shell elements (SAX2) for the wall was found to produce satisfactory results. No advantages were found in using higher order elements for the solid at the adopted mesh density.

[Insert Figure 5]

3. Effect of wall stiffness on computed stresses in the container

The effect of wall flexibility on silo pressures was studied before by Ooi and Rotter in the context of squat circular steel silos (Ooi and Rotter, 1990) and conical steel hoppers (Ooi and Rotter, 1991). The authors showed that in the range of wall stiffness expected in such structures, the wall provides sufficient confinement for the majority of industrial solids to remain predominantly in the pseudo-elastic state and the wall pressures are influenced by the relative stiffness of the solid wall interface. The authors proposed the parameter defined in Equation 3 to quantify this relative stiffness:

$$\alpha = \frac{E_s R}{E_w t} \qquad (3)$$

where E_s is the elastic modulus of the solid, R is the radius of the bin, E_w is the wall Young's modulus and t is the wall thickness. A higher value of α corresponds to a more flexible container.

The stiffness parameter α is adopted in this study to describe the wall flexibility of the container and a wide range of values is explored (Figure 2), corresponding to both highly flexible FIBCs and silos. The resulting wall pressures from the finite element computations are shown in Figure 6a. The wall flexibility has a significant effect on the wall pressure distribution both in the bin and hopper sections. The trend is characterised by a decrease of wall pressures in the bin, with a corresponding increase in the hopper as flexibility increases (as given by increasing α). In the hopper, a strongly increasing wall pressures towards the outlet region can also be observed with increasing wall flexibility.

[Insert Figure 6]

The corresponding regions of plastic flow and the vertical stress field in the stored solid are shown in Figure 7. The deformed shape of the container for all cases is shown without exaggeration.

At low and intermediate flexibility (α=0.01 and 0.5) the stored solid remains almost entirely in the elastic state, which concurs with the finding of Ooi and Rotter (Ooi and Rotter, 1990). However, in the case of high wall flexibility (α=2) the confinement provided by the wall is reduced sufficiently for a large portion of the solid to yield plastically in the bin section. In contrast, the solid in the hopper section remains entirely in the elastic state even at the high wall flexibility extreme.

The plastic flow in the bulk solid leads to a complex distribution of vertical stress (Figure 7b) characterised by non-uniformity on horizontal planes in the bin, which is contrary to Janssen's theoretical assumption (Janssen, 1895). Overall, there is a trend of diminishing arching within the solid in the bin with increasing wall flexibility and a corresponding increase of vertical stress towards the transition, contributing to significantly higher wall pressures in the hopper (Fig. 6a). Such large increases in pressure may have structural implications and may need to be taken into consideration for the structural design of highly flexible containers. Furthermore, the higher consolidation stresses near the outlet might result in higher cohesive strength of a cohesive solid and consequently exacerbate solid discharge problems in flexible containers, which is undesirable from an operational standpoint.

It is worth pointing out that changing the individual values of the wall and bulk solid Young's moduli did not change the computed wall pressures, if the value of the relative stiffness parameter α was maintained as shown in Figure 6b. This suggests that the numerical results for the very flexible cases in this study could also be relevant for much stiffer silos if a sufficiently stiff solid is stored in them.

[Insert Figure 7]

3.1 Stresses in the vertical bin section

The well-known Janssen equation (Eq. 4) has been adopted for the calculation of wall pressures in the bin section of silos in the relevant design codes around the world (e.g. AS 3774:1996, EN 1991-4:2006).

$$p = \frac{\gamma R}{2\mu}\left[1 - e^{-\frac{z_s}{z_0}}\right] \quad (4)$$

where $z_o = R/2mK$; z_s is the depth in the bin from a datum taken from one third of the height of the conical surcharge pile, R is the bin radius, μ is the coefficient of wall friction and K is the lateral pressure ratio (assumed constant with depth).

The application of Janssen's equation requires the selection of an appropriate value of the lateral pressure ratio K for the stored solid. Many theoretical values have been proposed and the important ones have been summarised by Ooi and Rotter (Ooi and Rotter, 1990). The analysis in this study focuses on the values proposed by Ooi and Rotter (Ooi and Rotter, 1990), Koenen (Koenen, 1895) and the value adopted in the Eurocode (EN 1991-4:2006). The aim of the analysis is to evaluate the relevant design code calculations, in which Janssen's theory is adopted, and gain insight into possible improvements in the case of highly flexible containers. The analysis is heuristic in nature and is not proposed in lieu of validation of the numerical model, for which published experimental measurements could not be identified.

Assuming a purely elastic bulk solid, Ooi and Rotter derived the value for the lateral pressure ratio shown in Equation 5, which also takes the flexibility of the silo wall into account.

$$K_e = \frac{v_s}{1 - v_s + \alpha} \quad (5)$$

Where υ_s is the Poisson ratio of the bulk solid and α is the relative stiffness parameter from Equation 3.

At the opposite extreme Koenen assumed that the material is yielding plastically everywhere in the solid and derived the expression for K in Equation 6 on the basis of the Rankine active state.

$$K = \frac{1 - \sin(\phi)}{1 + \sin(\phi)} \quad (6)$$

where φ is the effective angle of internal friction of the solid.

It should be noted that in this study, the Poisson ratio for the bulk solid is related to the Eurocode value of K through Equation 1. A substitution of this equation into Ooi and Rotter's calculation (Equation 5) reveals that the latter differs from the Eurocode only by the inclusion of the parameter α. Consequently the two calculations are quite similar when α is small (a very stiff wall).

A comparison between the corresponding theoretical pressure distributions and the numerical results is shown in Figure 8a. At the high wall stiffness extreme (α=0.01) the solid remains entirely in the elastic state, corresponding to the conditions assumed by Ooi and Rotter and adopting their proposed K_e=0.39 yields a reasonably good prediction of the wall pressure away from the hopper transition. In this case the Eurocode calculation gives quite similar distribution as explained above. The agreement with Ooi and Rotter's prediction of a reduced pressure distribution is still good at an intermediate wall stiffness of α=0.5, where K_e=0.23 – this is not present in the Eurocode calculation since wall flexibility is not considered. At higher wall flexibility, however, the results move away from the theoretical predictions and seemingly away from the shape of the Janssen pressure distribution. This can be explained by the significant variation in the computed

lateral pressure ratio with depth as shown in Figure 8b. The variation is characterised by a continuous decrease toward the transition with the hopper and is in contrast with the theoretical assumption of a constant value for K. An examination of the vertical and shear stress distributions in the bin for the pair of stiff (α=0.01) and very flexible container (α=2.0) in Figure 9 reveals the cause.

[Insert Figure 8]

[Insert Figure 9]

The plastic flow induced by the high wall flexibility leads to a redistribution of stresses in the solid, characterised by a transfer of vertical stress away from the wall and towards the centre of the bin as shown in Figure 9 a and b. The redistribution is caused by the developing rupture regime, giving rise to a reversal of the arching in the solid as evidenced by the decrease in shear stress (Figure 9 c and d). Consequently, the stresses carried by the wall are decreased and there is corresponding overall increase in the mean vertical stress towards the transition. The combination of decreased stresses at the wall and an increasing mean vertical stress leads to the observed reduction in the computed lateral pressure ratio K with depth at high wall flexibility.

Evidently, plasticity has a large influence on the computed stresses in the bin, but the extent of plastic flow depends on the effective angle of internal friction of the solid. Therefore, it is worth examining the effect of this parameter on the computed stresses. The results for a wide range of values of the effective angle of internal friction are shown in Figure 10 and the corresponding regions of plastic flow and vertical stress distributions are shown in Figure 11. Only the results for the most flexible container are shown, because the effect in this case is most pronounced.

[Insert Figure 10]

[Insert Figure 11]

The angle of internal friction has significant effect on the computed wall pressures and the relationship is characterised by a variation between the theoretical predictions of Ooi and Rotter and Koenen respectively (Figure 10a). At the very high internal friction of $\varphi=60^0$, the solid remains in the elastic state even at the high degree of wall flexibility considered (Figure 11a). The corresponding pressure distribution is characterised by a constant value of K with depth (Figure 10b) and conforms to Ooi and Rotter's elastic prediction (Figure 10a). At intermediate values of internal friction ($\varphi=30\text{-}50^0$) a partial yielding of the solid in the bin leads to a complex state of stress characterised by a variation of K with depth and a deviation of the wall pressure distribution from Janssen's equation as discussed previously. At the low internal friction of $\varphi=25^0$, nearly all of the solid is in a plastic state (Figure 11a). This leads to a reduction in shear stress in the solid and a return to a more uniform vertical stress distribution as shown in Figure 12a. As a result the value of K is nearly constant with depth. These conditions correspond to the active-plastic condition proposed by Koenen for the lateral pressure ratio and the computed pressures agree well with the Koenen's theoretical prediction.

[Insert Figure 12]

These results suggest that the wall pressure in a very flexible container is governed by plasticity and that the extent of the plastic yielding is influenced by the interplay of wall stiffness and internal angle of friction of the solid. An examination of the mean value of the computed lateral pressure ratio for the whole bin, shown in Figure 13, reveals this relationship. In all wall stiffness cases the mean lateral pressure ratio K decreases to a constant value as the internal friction angle of the solid increases. The decrease of the mean K with increasing angle of internal friction indicates that the solid is yielding

plastically, while a constant value indicates a solid in the elastic state. For a stiff wall (α=0.01) the solid remains in the elastic state for all but a low friction angle solid ($\varphi<30^{o}$), which is in agreement with Ooi and Rotter's results (Ooi and Rotter, 1990). However, the range of internal friction angles for which plasticity affects the results increases with the wall flexibility and extends even to highly frictional solids ($\varphi>50^{o}$) as the relative stiffness parameter increases (α=2). In addition, as shown previously, when the solid yields plastically the lateral pressure ratio K significantly deviates from a constant value with depth (Figure 10b). This variation produces a wall pressure distribution, which is complex and does not conform to the Janssen distribution (Figure 10a). Therefore, a description of the variation of K with depth in terms of the solid and wall material parameters might be needed for an improved prediction of the wall pressure distribution in the bin of a highly flexible container.

[Insert Figure 13]

3.2 Stresses in the hopper section

Many theories have been proposed for the static and flow wall pressures in the hopper section of silos. The most important ones have been compiled by Arnold et al. (1980). In this study, the FE analysis will be compared with the Walker theory (Walker, 1966), which is adopted in the Eurocode (EN 1991-4:2006) for both the static and flow cases. It is based on the differential slice method (similar to Janssen's theory). For an axisymmetric hopper, the normal wall pressure in Walker's theory takes the form:

$$p = FD\left(\frac{\gamma H}{n-1}\right)\left(\left(\frac{H-z}{H}\right)-\left(\frac{H-z}{H}\right)^{n}\right)+\sigma_{zt}\left(\frac{H-z}{H}\right)^{n} \quad (7)$$

where $n = 2(FD\mu\cot(\beta) + FD - 1)$, γ is the unit weight of the solid, μ is the coefficient if wall friction, β is the hopper half angle, H is the height of hopper, z is the depth below the transition with the bin, σ_{zt} is the vertical surcharge stress at the transition, F is the hopper pressure ratio and D is the stress distribution factor.

The stress distribution factor D (the ratio of mean vertical stress to vertical stress at the wall on any horizontal plane) is assumed by Walker to be unity in all cases. Consequently, this parameter is not included in the Eurocode equation. However, it is included here to aid the discussion. The hopper pressure ratio F (the ratio between the mean vertical stress and wall pressure) is assumed to be different for the static and flow cases. The corresponding Eurocode equations are shown below (Equations 8 and 9).

$$F_{static} = 1 - \frac{b}{1 + \tan(\beta)/\mu} \tag{8}$$

$$F_{flow} = \frac{1 + \sin(\phi)\cos(\epsilon)}{1 - \sin(\phi)\cos(2\beta + \epsilon)}\ ;\ \epsilon = \phi_w + \operatorname{asin}\left(\frac{sin(\phi_w)}{sin(\phi)}\right)\ ;\ \phi_w = \operatorname{atan}(\mu) \tag{9}$$

where φ is the effective angle of internal friction of the solid, β is the hopper half angle and b is an empirical parameter taken as 0.2 according to the Eurocode.

The computed wall pressure distributions in the hopper section at varying degrees of wall flexibility are shown in Figure 14a along with the theoretical predictions. It should be noted that the vertical surcharge stress (σ_{zt}) used in the theoretical calculation was the mean value calculated from the four wall stiffness cases.

[Insert Figure 14]

The Eurocode calculation yields very similar results for the static and flow cases with corresponding FD values of 0.95 and 0.92 respectively. These values are close to unity as suggested by McLean (McLean, 1985) and yield reasonably good predictions at the high

wall stiffness situation (α=0.01). At higher wall flexibility, however, the computed wall pressure distribution changes markedly and is characterised by a transfer of pressure towards the outlet. An overall decrease in the computed hopper pressure ratio FD with decreasing wall stiffness can be observed as shown in Figure 14b. Consequently, adopting lower values for FD in Walker's equation yields an improved prediction in cases of high wall flexibility (Figure 14a). However, in such cases (α≥0.5) there is a significant variation of FD with depth and the use of a single value is questionable. Furthermore, the computed values of F and D vary with depth individually in the hopper as shown in Figure 15, which poses a further challenge.

[Insert Figure 15]

[Insert Figure 16]

The vertical and shear stress distributions at the two wall flexibility extremes are shown in Figure 16. In the stiff-walled case the vertical stress distribution is approximately uniform on horizontal planes (Figure 16a) and is characterized by a monotonic decrease towards the outlet. There is an associated arching action within the solid as evidenced by the shear stress distribution, shown in Figure 16c. With the highly flexible wall, significantly higher vertical stresses can be observed throughout the hopper with a higher surcharge stress at the transition partially contributing to this increase (Figure 16b). In contrast with the stiff-walled case, the vertical stress increases towards the outlet and a transfer of stress away from the wall and towards the middle of the hopper can be observed. There is an associated reduction of arching within the stored solid, as evidenced by the reduction of shear shown in Figure 16d.

With respect to Equation 7, the radially uniform vertical stress distribution in the stiff-walled case leads to values of the stress distribution factor D close to unity throughout the

hopper, as assumed by Walker (Figure 15a). The modest increase above unity is due to the arching action in the solid leading to a small increase of vertical stress at the wall. With the highly flexible wall, the redistribution of stress towards the middle of the hopper leads to a significant reduction of the distribution factor D (Figure 15a) especially near the transition. As the radial stiffness of the hopper wall increases towards the outlet, so does the stress distribution factor. Consequently, a return to the values for the stiff-walled case is observed near the outlet. The stiffening of the hopper wall with depth could also explain the observed increase in hopper pressure factor F near the outlet as shown in Figure 15b, since the solid in the hopper remains in the elastic state for all but a very free flowing solid (Figure 10a).

As discussed before, the observed significant increases in the computed stresses in the hopper of a very flexible container might have negative implications from both a structural and operational standpoint and a more accurate theoretical description of these stresses might be needed for an improved design. It appears that such a description will require the development of expressions for both the vertical stress distribution factor D and the hopper pressure ratio F in terms of the material and geometric parameters and this could form the basis of future work.

Lastly, the change in the hopper geometry at low wall stiffness should be mentioned. In this study, the induced curvature in the hopper was negligible (the slope varied less than 1 degrees) even at the lowest wall stiffness (α=2). This might not be the case if the stiffness is decreased further and the effect of the change in hopper curvature might also need to be explored in the future.

4. Conclusions

A finite element study of the effect of wall stiffness on the stresses in a flexible-walled axisymmetric container storing bulk solids has been presented. The results show that highly flexible walls lead to a significant redistribution of stresses in the container, characterized by a transfer of wall pressure from the vertical bin section to the hopper section and an associated increase of vertical stress throughout the stored solid in the container. In the case of a typical industrial flexible container, the maximum vertical stress in the solid could increase by as much as 300% compared to a stiff-walled silo and is accompanied by large increase of pressure on the hopper wall. Since the maximum load on the hopper is one of the principal load cases for the structural design of silos (Eurocode EN 1991-4:2006), such large increases may need to be taken into consideration in the structural design of flexible containers. Currently wall flexibility is not considered in the Eurocode and the computed wall pressure distributions in both the hopper and bin section in this analysis differ significantly from the respective design code calculations. It should also be pointed out that the higher consolidation stresses in the bulk solid can lead to increased bulk strength in the case of cohesive solids, which may in turn exacerbate operational problems such as incomplete or arrested discharge.

It is found that the computed stresses in the vertical bin section of a flexible container are strongly influenced by plasticity in the stored solid. The extent of plastic yielding is determined by the interplay of wall flexibility and the effective angle of internal friction of the solid. Both an entirely elastic and entirely plastic state are possible for the solid at practical extremes of the internal friction angle ($\varphi=60^{o}$ and $\varphi=25^{o}$ respectively) with partial yielding occurring in the intermediate range. If the solid is sufficiently frictional to remain in the elastic state, Janssen's equation describes the computed wall pressure

distribution well when Ooi and Rotter's elastic lateral pressure ratio is adopted (Ooi and Rotter, 1990). At the opposite extreme of a very free flowing solid entirely in the plastic state, the computed pressure distribution is well described by employing Koenen's lateral pressure ratio (Koenen, 1895) based on the Rankine active state of failure. In all other cases, partial yielding in the solid leads to a complex state of stress, characterized by a large variation of the lateral pressure ratio K with depth, which is in contrast with Janssen's theoretical assumption. Consequently, the computed wall pressure distribution in these cases does not conform to the Janssen pressure distribution, suggesting that an improved prediction will require a description of the variation of K with depth in terms of the solid and wall material parameters.

In contrast with the bin section, the solid in the hopper section remains predominantly in the elastic state even at high wall flexibility (α=2) and for all but extremely flowable bulk solids (φ=25°). It is found that Walker's flow theory provides a qualitative description of the computed wall pressures in the hopper, when appropriate values of the distribution factor *D* and hopper pressure ratio *F* are used. The values for these parameters given by the Eurocode (EN 1991-4-2006) provide a good description of the wall pressure for stiff walled containers, but the computed F and D values are found to decrease as wall flexibility increases, which is not reflected in the design code. These parameters are also computed to vary significantly with depth in the hopper.

Acknowledgements

The authors are grateful to Dr Prashant Gupta, Dr Luis Martin de Juan and Dr Hossein Ahmadian of Procter and Gamble for their assistance and useful discussions regarding flexible bulk containers.

Declaration of conflicting interests

The Authors declare that there is no conflict of interest.

Funding

This work was supported by the Engineering and Physical Sciences Research Council and Procter and Gamble Co. through an industrial CASE award.

References

Arnold P, McLean A and Roberts A (1980) Bulk Solids: Storage, Flow and Handling. Australia: Tunra Bulk Solids Handling Research Associates, University of Newcastle.

AS 3774:1996 (1996) Loads on bulk solids containers. Standards Association of Australia.

Chen JF, Yu SK, Ooi JY, et al. (2001) Finite-Element Modelling of Filling Pressures in a Full-Scale Silo. Journal of Engineering Mechanics 127(October): 1058–1066.

Ding S, Rotter JM, Ooi JY, Enstad G, Xu D, Normal pressures and frictional tractions on shallow conical hopper walls after concentric filling: Predictions and experiments. Chemical Engineering Science 89:264-272.

Dinh TD, Rezaei A, Puystiens S, et al. (2015) A study of tension fabric membrane structures under in-plane loading: Nonlinear finite element analysis and validation. Composite Structures, Elsevier Ltd 128: 10–20.

EN ISO 1421:1998 (1998) Rubber or plastics coated fabrics - Determination of tensile strength and elongation at break. Comité Européen de Normalisation.

EN 1991-4:2006 (2006) Eurocode 1- Actions on structures – Part 4: Silos and Tanks. Comité Européen de Normalisation.

Feise H and Schwedes J (1998) Constitutive laws for granular materials. In: Silos: Fundamentals of theory behaviour and design. London: Spon Press, p. 528.

Goodey RJ, Brown CJ and Rotter JM (2003) Verification of a 3-dimensional model for filling pressures in square thin-walled silos. Engineering Structures 25(14): 1773–1783.

Goodey RJ, Brown CJ and Rotter JM (2006) Predicted patterns of filling pressures in thin-walled square silos. Engineering Structures 28(1): 109–119.

Hallal A, Younes R and Fardoun F (2013) Review and comparative study of analytical modeling for the elastic properties of textile composites. Composites Part B-Engineering 50: 22–31.

Häussler U and Eibl J (1984) Numerical investigations on discharging silos. Journal of Engineering Mechanics 110(6): 957–971.

Holst JMFG, Ooi JY, Rotter JM, et al. (1999) Numerical modelling of silo filling. I: Continuum analysis. Journal of Engineering Mechanics 125(1): 94–103.

Janssen HA (1895) Versuche über Getreidedruck in Silozellen. Zeitschrift des Vereines Deutscher Ingenieuere 39(35).

Koenen M (1895) Berechnung des seitenung bodendrucks in silos. Zentralbl. Bawenwaltung 16: 446–449.

Link RA and Elwi AE (1990) Incipient flow in silo-hopper configurations. Journal of Engineering Mechanics 116(1): 172-188.

McLean AG (1985) Initial stress field in converging channels. Bulk Solids Handling 5(2): 49–54.

Nielsen J and Wedner J (1998) The choice of constitutive laws for silo media. In: Silos: Fundamentals of theory behaviour and design. London: Spon Press, p. 539.

Ooi JY (1990) Bulk solids behaviour and silo wall pressures. PhD Thesis, University of Sydney, Australia.

Ooi JY and Rotter JM (1990) Wall pressures in squat steel silos from simple finite element analysis. Computers & Structures 37(4): 361–374.

Ooi JY and Rotter JM (1991) Elastic predictions of pressures in conical silo hoppers. Engineering Structures 13(1): 2-12.

Ooi JY, Pham L and Rotter JM (1990) Systematic and random features of measured pressures on full-scale silo walls. Engineering Structures 12: 74–87.

Ooi JY, Chen JF, Lohnes RA, et al. (1996) Prediction of static wall pressures in coal silos. Construction and Building Materials 10(2): 109–116.

Pargana JB, Lloyd-Smith D and Izzuddin BA (2007) Advanced material model for coated fabrics used in tensioned fabric structures. Engineering Structures 29(7): 1323–1336.

Rotter JM (2001) Guide for the economic design of circular metal silos. London: Spon Press.

Simulia (2012) Abaqus Analysis: User's Manual. Dassault Systemès.

Simulia (2012) Chapter 4.4.5. In: Abaqus Theory Manual. Dassault Systemès.

Tejchman J (1998) Numerical simulation of filling in silos with a polar hypoplastic constitutive model. Powder Technology 96: 227-239.

Walker DM (1966) An approximate theory for pressures and arching in hoppers. Chemical Engineering Science 21: 975–997.

Wang Y, Lu Y and Ooi JY (2013) Numerical modelling of dynamic pressure and flow in hopper discharge using the Arbitrary Lagrangian-Eulerian formulation. Engineering Structures 56: 1308–1320.

Wójcik M and Tejchman J (2009) Modeling of shear localization during confined granular flow in silos within non-local hypoplasticity. Powder Technology 192:298-310.

Wójcik M and Tejchman J (2016) Buckling analyses of metal cylindrical silos containing bulk solids during filling. Particulate Science and Technology 34:461-469

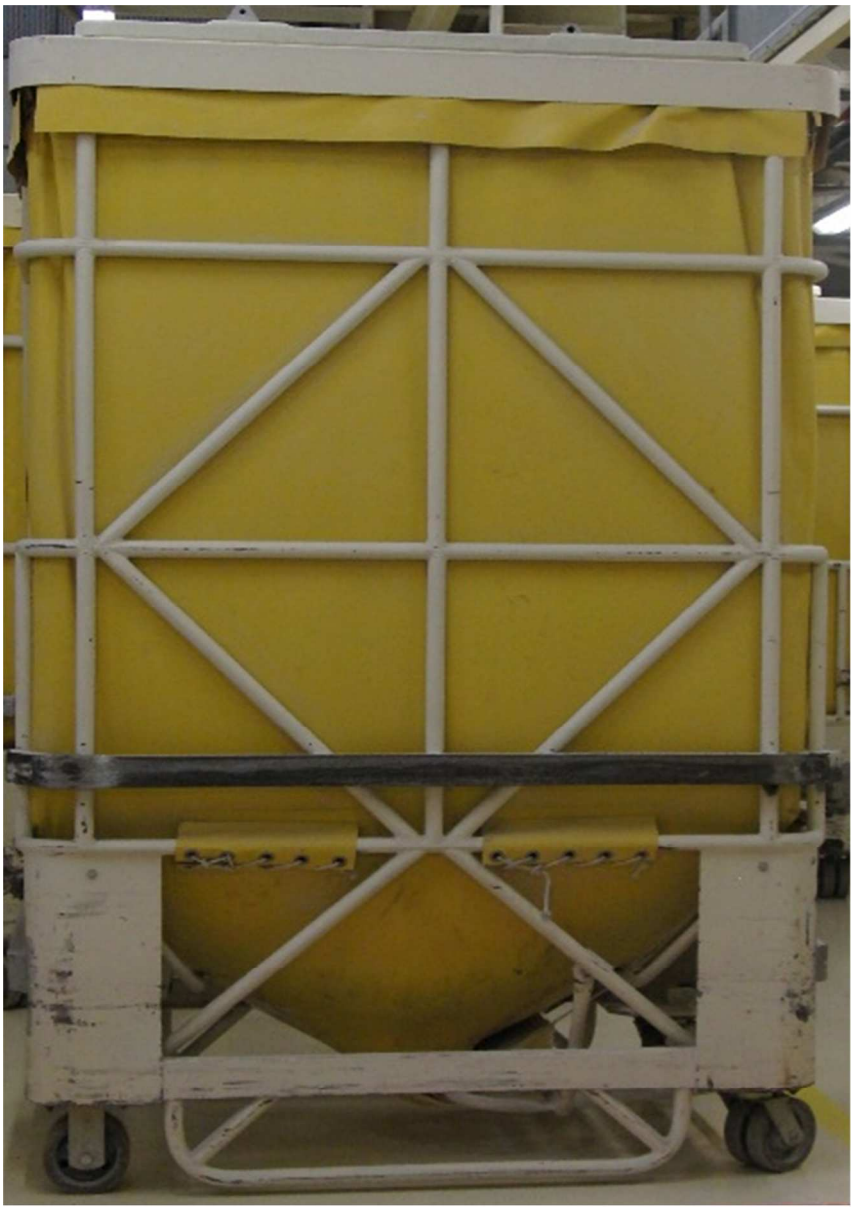

Figure 1 A typical flexible container for storage and transport of powders, called a “buggy”.

90x127mm (300 x 300 DPI)

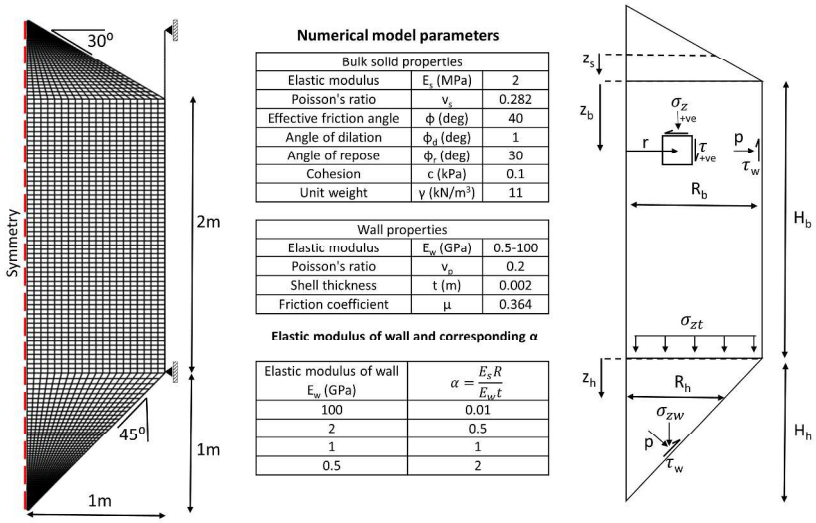

Figure 2 Container geometry, FE mesh, boundary conditions, numerical model parameters and notation.

338x190mm (300 x 300 DPI)

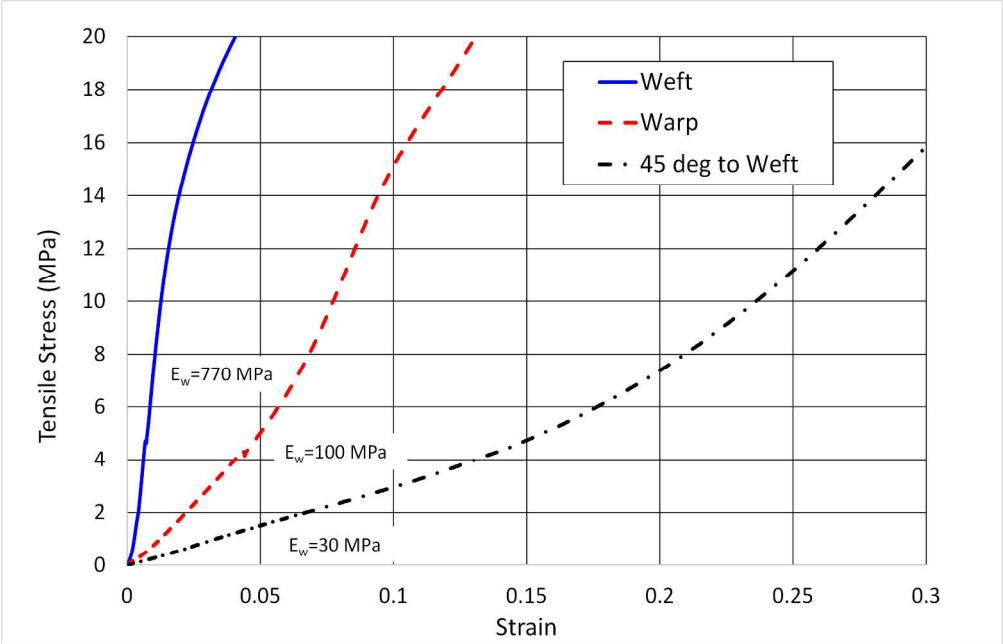

Figure 3 Stress-strain curves for the powder buggy wall canvas from uniaxial extension tests in three directions.

242x156mm (300 x 300 DPI)

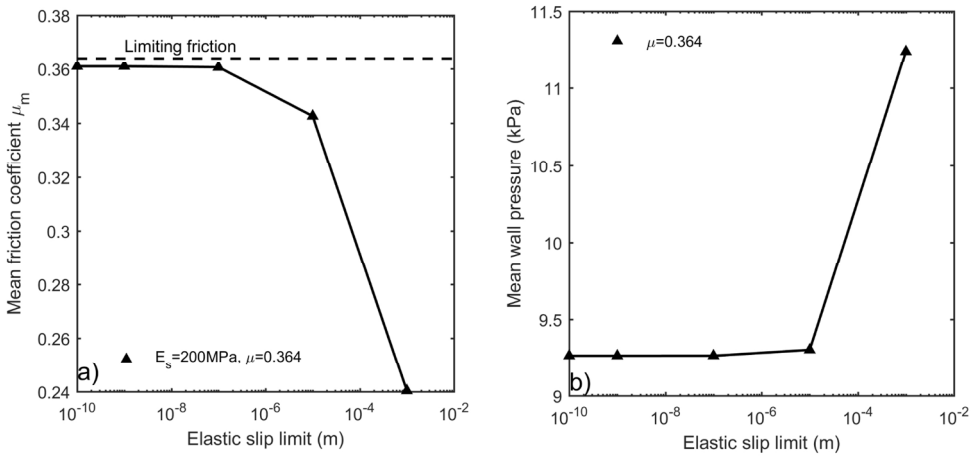

Figure 4 Effect of elastic slip on a) the friction mobilisation along the wall; and b) the computed wall pressures.

212x106mm (300 x 300 DPI)

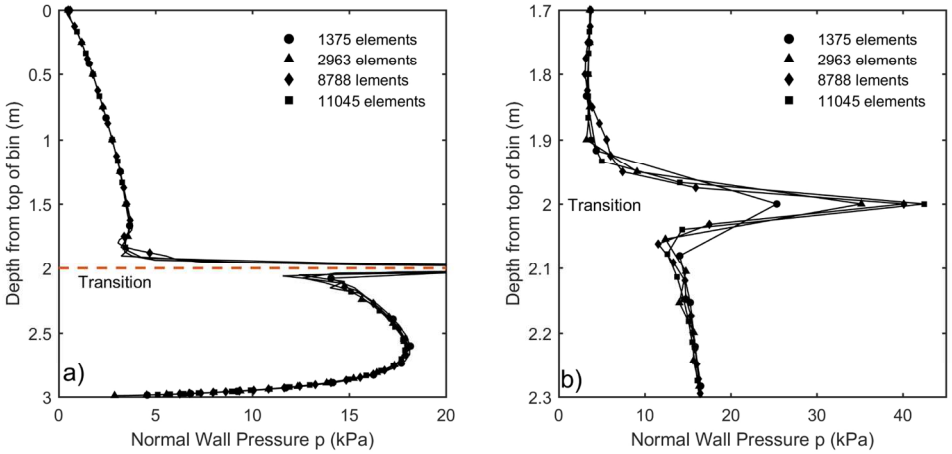

Figure 5 Effect of mesh density on a) the computed wall pressures in the container and b) the computed pressure peak at the transition.

212x106mm (300 x 300 DPI)

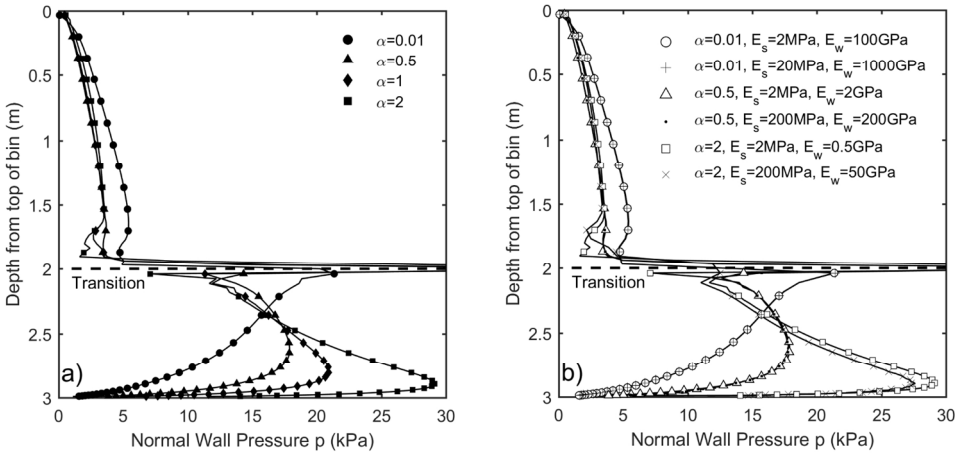

Figure 6 Normal wall pressure at a) varying bulk solid-wall stiffness and b) at the two bulk solid-wall stiffness extremes with varying Young's moduli for the bulk solid and wall.

212x106mm (300 x 300 DPI)

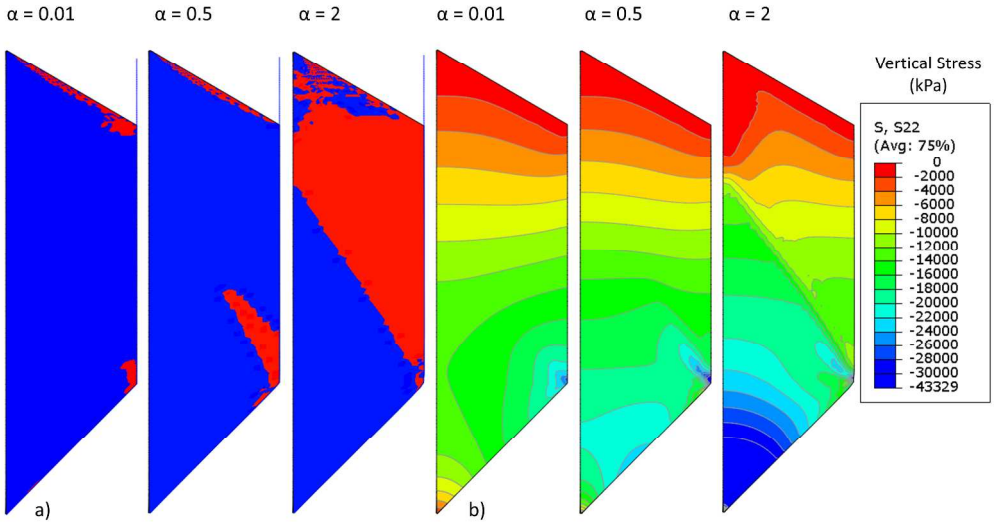

Figure 7 a) Regions of plastic flow (red) in the bulk solid and b) vertical stress contours at varying bulk solid-wall stiffness.

338x190mm (300 x 300 DPI)

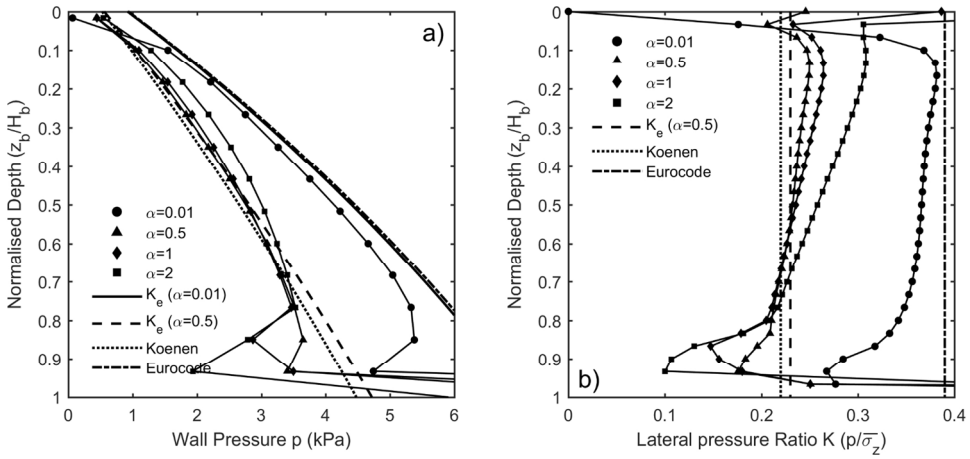

Figure 8 a) Normal wall pressure and b) lateral pressure ratio in the bin at varying bulk solid-wall stiffness.

212x106mm (300 x 300 DPI)

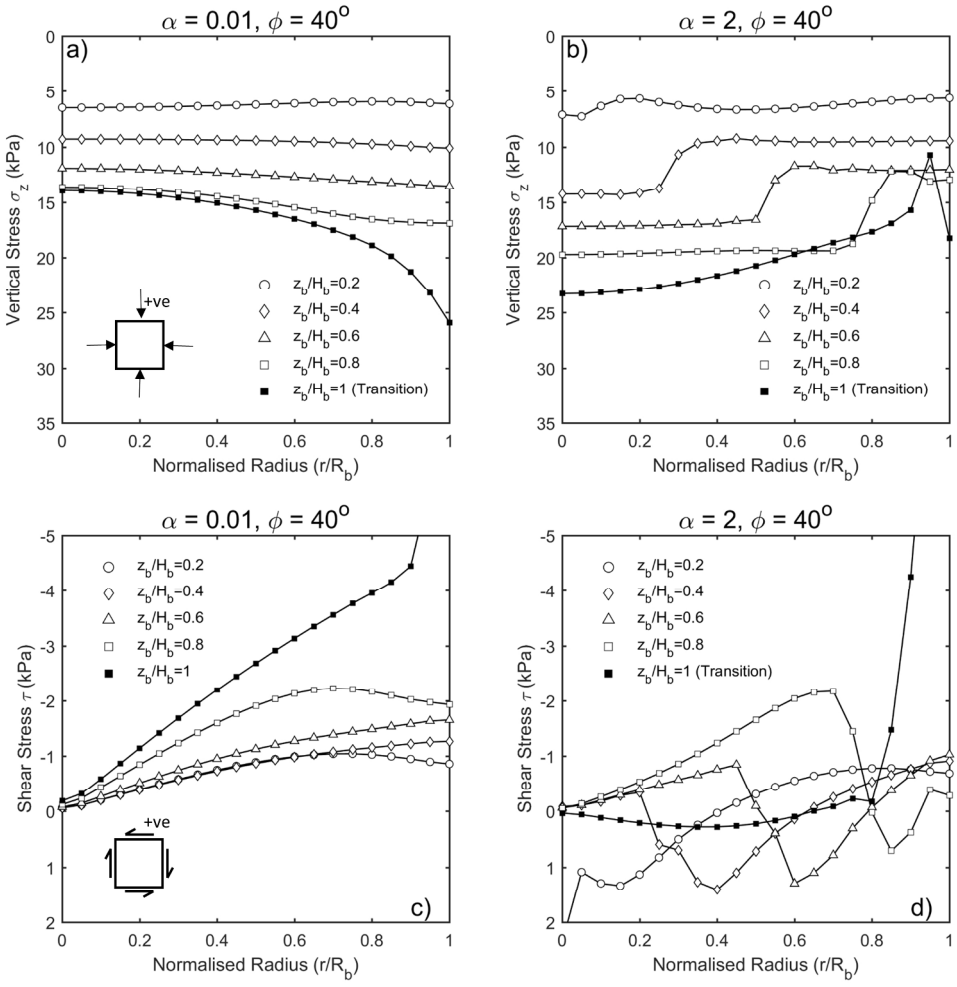

Figure 9 Vertical and shear stress distributions at varying depths in the bin at the two wall stiffness extremes.

212x212mm (300 x 300 DPI)

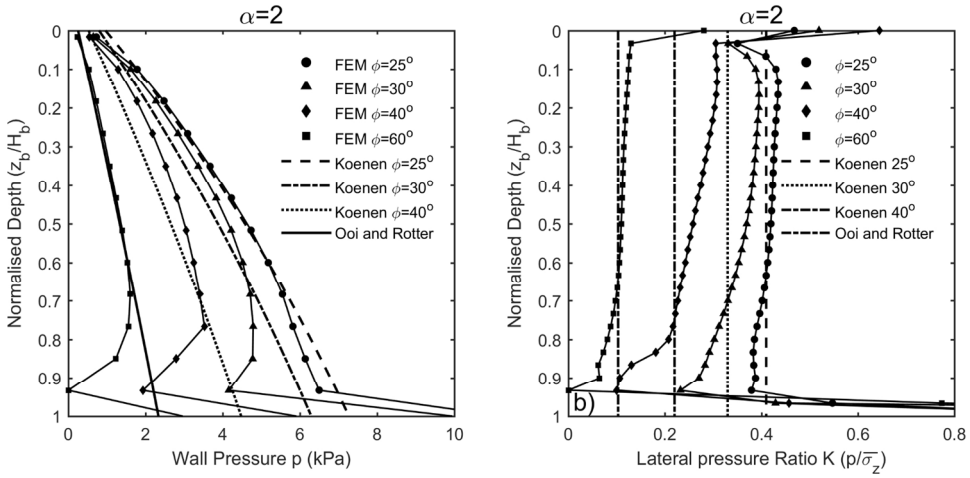

Figure 10 a) Normal wall pressure and b) lateral pressure ratio in the bin at the high wall stiffness extreme with varying effective angle of internal friction for the solid.

212x106mm (300 x 300 DPI)

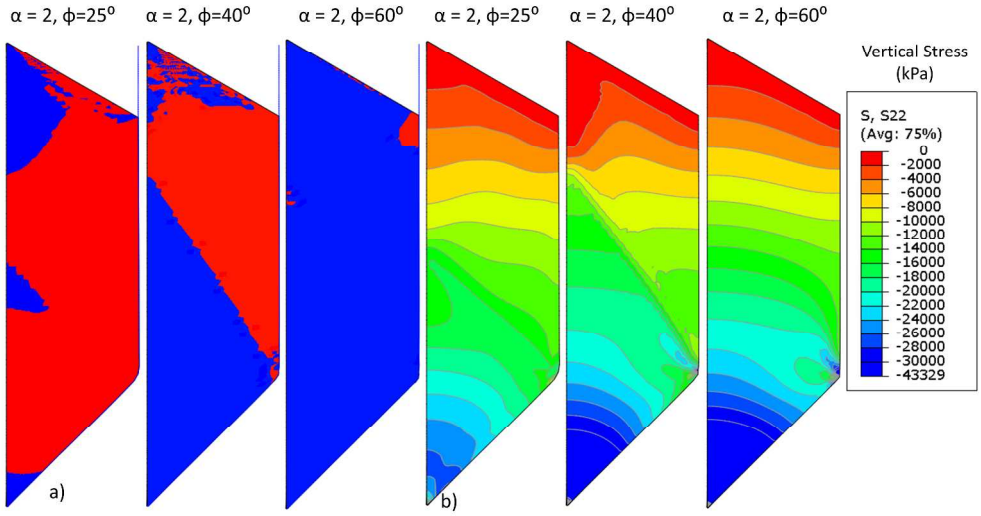

Figure 11 a) Actively yielding regions (red) in the bulk solid and b) vertical stress contours at varying effective angle of internal friction.

338x190mm (300 x 300 DPI)

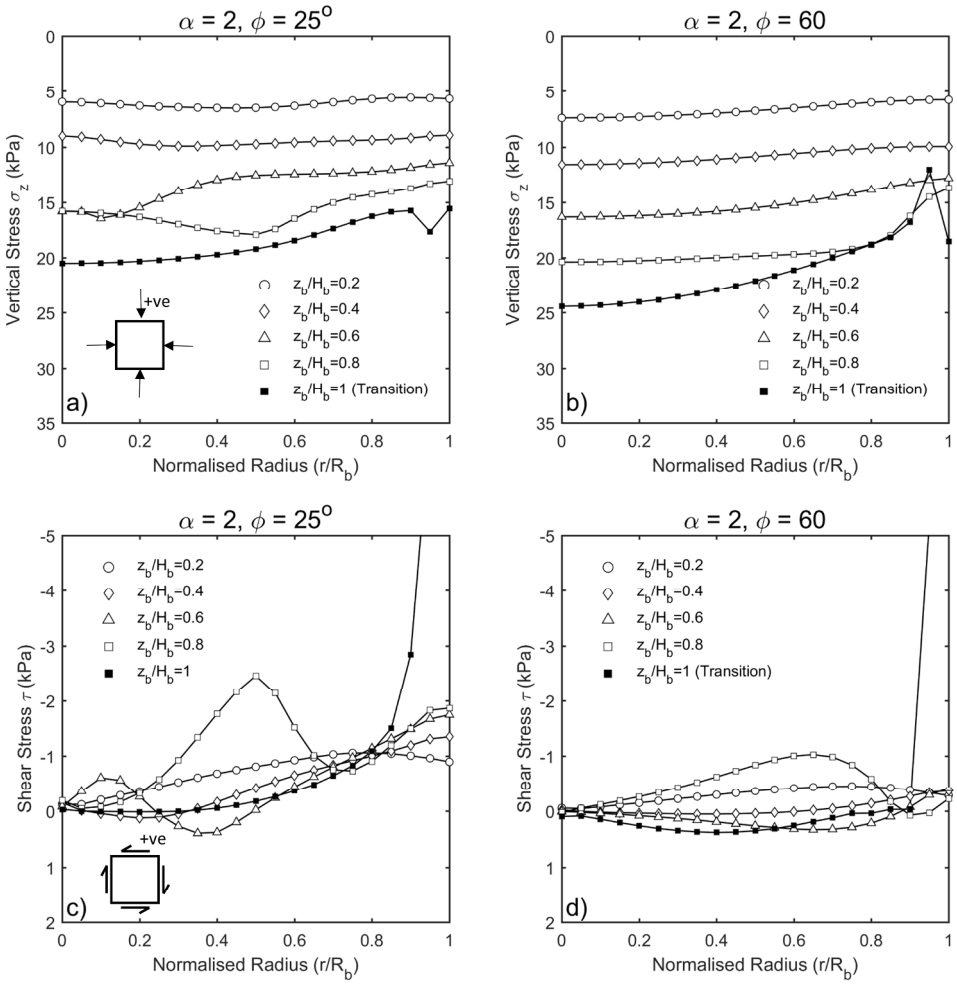

Figure 12 Vertical and shear stress distributions at varying depths in the bin at two extremes of the effective angle of internal friction of the solid.

212x212mm (300 x 300 DPI)

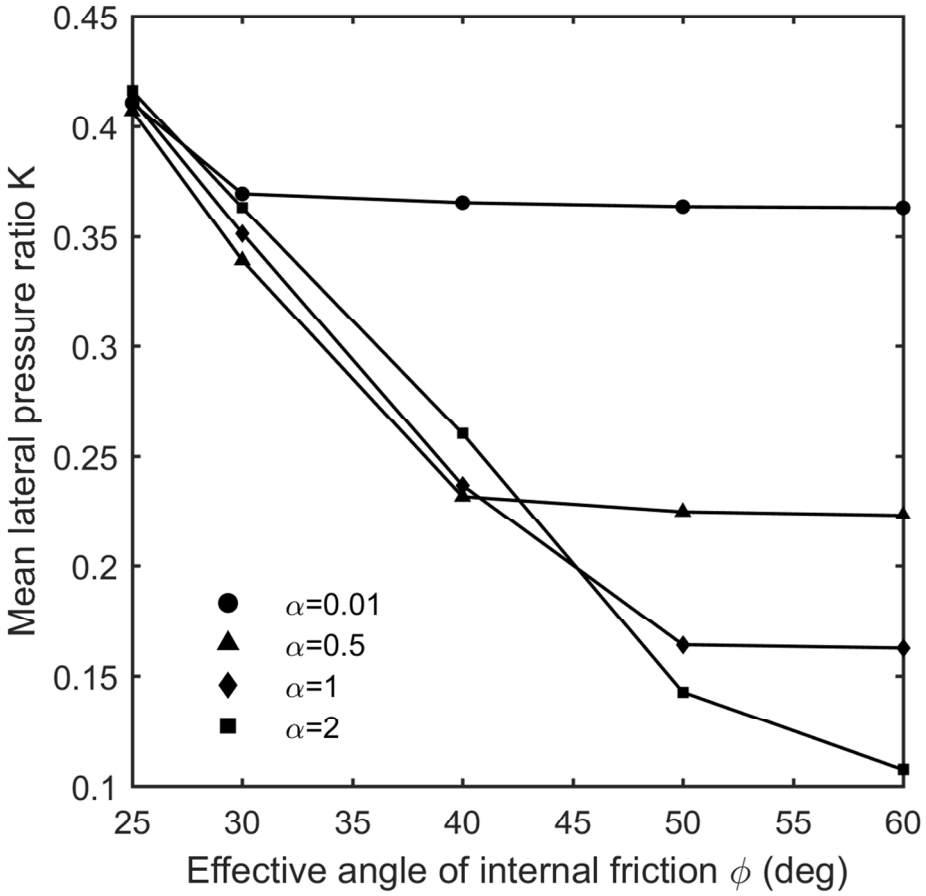

Figure 13 Variation of the mean lateral pressure ratio K in the bin with the angle of internal friction of the solid and the relative bulk solid-wall stiffness.

105x105mm (300 x 300 DPI)

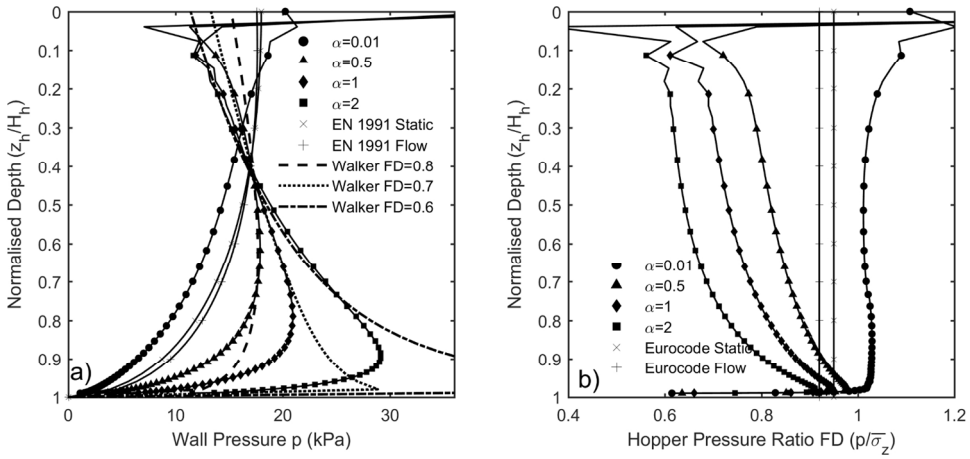

Figure 14 a) Normal wall pressure in the hopper and b) hopper pressure ratio at varying bulk solid-wall stiffnesses.

212x106mm (300 x 300 DPI)

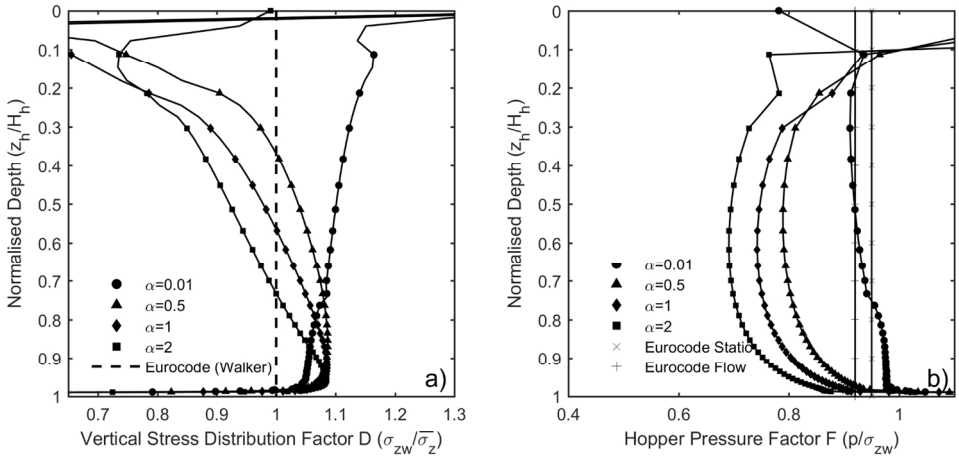

Figure 15 a) Vertical stress distribution factor and b) hopper pressure factor at varying bulk solid-wall stiffnesses.

212x106mm (300 x 300 DPI)

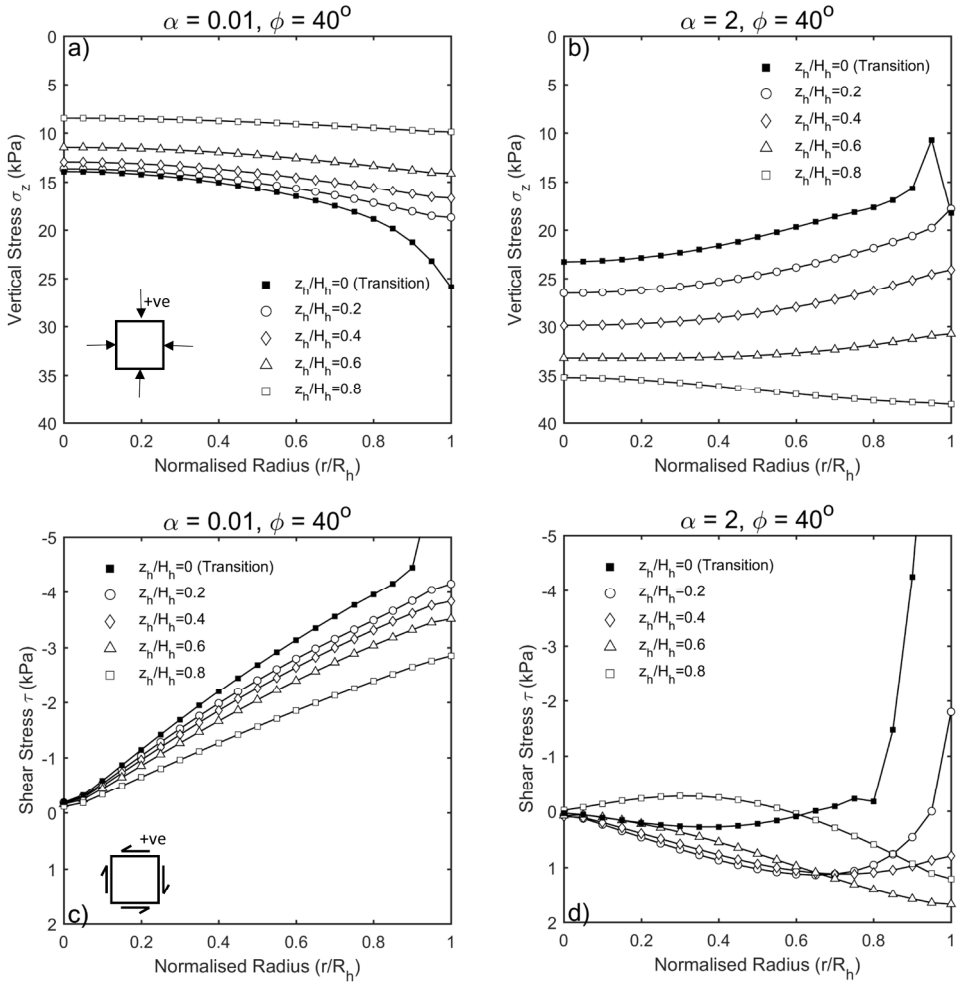

Figure 16 Vertical and shear stress distributions in the hopper at the two solid-wall stiffness extremes.

212x212mm (300 x 300 DPI)